2001-01-1553

Dynamic Interactions Between Loaded and Unloaded Gear Pairs Under Rattle Conditions

T. C. Kim and R. Singh
The Ohio State Univ.

ABSTRACT

In many manual transmissions, conditions for the onset of vibro-impacts from an unloaded gear pair are more likely than from an engaged set. Although some of the general characteristics of neutral gear rattle are known, no specific analytical models are available in the literature that can explain interactions between unloaded and loaded gear pairs in the drive rattle mode. For the sake of illustration, a particular problem for a light duty truck is studied in this paper and dynamic interactions are investigated. Some experimental measurements are first presented to define the unloaded gear rattle problem. Linear and non-linear mathematical models of the driveline are developed to understand, quantify and control the rattle problem. Trends predicted by simulations are compared with those observed in experiments. The effects of various gear run-ups and vibratory drag torques are investigated.

INTRODUCTION

Vibro-impacts are induced by gear backlashes and other clearance non-linearities in many drive systems including manual transmissions of cars and trucks. These vibro-impacts lead to excessive vibration, noise, and dynamic loads, and could pose fatigue, reliability, and customer satisfaction issues. Current vehicle design trends toward lighter flywheels and lower idling speeds increase the likelihood of introducing gear rattle as a major noise source, especially from the perceived sound quality standpoint. In some cases, unloaded pairs rattle in the drive mode since the load carried by an unengaged gear pair is light and yet it may be dynamically excited. Therefore, the onset of vibro-impacts from unloaded gear pairs or splines seem to be more favorable than rattle from an engaged gear pair.

Prior investigators have used a variety of simulation techniques to understand and predict such problems [1-5]. Although some of the general characteristics of neutral gear rattle in automotive transmissions are investigated [1-7], no specific analytical models are available which explain the dynamic behavior of an unloaded gear pair in the drive rattle mode [8]. In this paper, an experimental study is briefly described, and a typical unloaded gear rattle case is examined. Next, two mathematical simulation models are proposed. Typical results from numerical simulation are discussed and compared with those from the experiments. Furthermore, various conditions for viscous drag torque between the unloaded gear and output shaft will be investigated as well as the effect of viscous drag torque distribution.

EXPERIMENTAL CASE STUDY

Consider an unloaded gear pair rattle problem that occurs in a certain vehicle whose specifications are listed in Table 1. The schematic of this transmission is represented in Figure 1 via a lumped parameter torsional model. Initial experiments are conducted on transmission A to clarify the rattle phenomenon in a qualitative manner. Then, all measurements are compared with a benchmark transmission (B) and differences between alternate rattle problems are noted. Experiments under varying conditions show that significant and annoying rattle noises are produced by transmission A at lower engine speeds during light accelerations or coast conditions. Nonetheless, the rattle noise can be heard in all engaged gear run-ups.

Torsional velocity ($\dot{\theta}$, rpm) time histories are acquired via running this vehicle in first, second, and third gear run-ups. Subsequently, the velocity ($\dot{\theta}$) data are converted into accelerations ($\ddot{\theta}$). The third, sixth, and ninth engine firing orders are removed in order to clearly observe impulsive signals. Summary of results for the relative acceleration levels ($\ddot{\theta}_p$) on a peak-to-peak basis are shown in Table 2. In addition, some relative, and translational acceleration levels along the line of meshing action ($\ddot{\delta}_p$) are shown in Table 2. Experiment clearly shows that the main rattle noise comes from the

unloaded gear pairs since acceleration levels between engaged and unloaded pairs are significant. Especially for this transmission, the $\ddot{\theta}_p$ level of the overdrive (unloaded) gear pair is much higher than those from the other unloaded gears, say during the first or second gear run-ups. Such phenomena occur in all gear run-up conditions. Similar trends are also detected in the benchmark transmission (B) experiment, but the severity of rattle, say in terms of relative acceleration levels, is lower than transmission A.

From the viewpoint of source-path-receiver network, the rattle noise source appears to be dominant. Measured spectral characteristics between the casing acceleration and radiated sound are different. This seems to suggest that the role of the housing is minimal. Therefore, examination of dynamic paths is beyond the scope of this work. It is concluded that the main source of sound is the vibro-impacts from one or more gear pairs. However, the nature of the underlying physical phenomena, including which gear pair initiates vibro-impacts and whether single-sided or double-sided impacts are generated, can not be understood based on the experimental study alone. Therefore, mathematical simulation models must be developed.

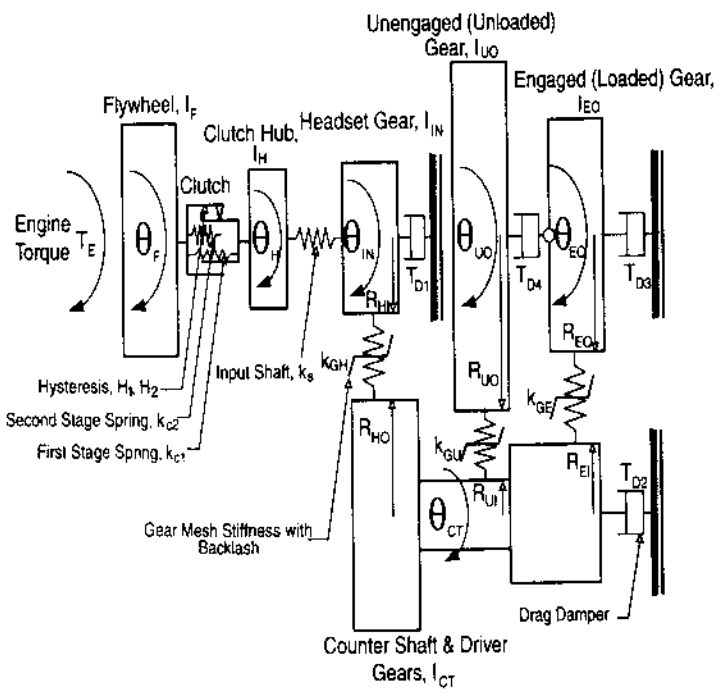

Figure 1. Typical non-linear simulation model for gear rattle analysis

LINEAR SIMULATION MODEL

Figure 1 shows schematically a generic torsional model of a dual-axis type automotive manual transmission. It has been shown that lumped parameter model approach is sufficient to study phenomena under the neutral, light acceleration, or coast rattle problems [1-6]. In order to specifically study the relationship between engaged and unloaded gear pair rattle, the scope of model is limited a sub-set of the drivetrain, from the flywheel to the output shaft as shown in Figure 1. As a first step in model development, a linear time-invariant (LTI) model of Figure 1 is proposed with the following assumptions. First, the clutch is assumed linear with the first stage clutch spring stiffness (k_{c1}) without any hysteresis. Second, each shaft acts like a linear torsional spring (k_s). Third, the gear interface regime may be modeled by an equivalent mesh stiffness term [3]. Relevant inertial elements are defined by the flywheel and clutch friction pad (I_F), clutch hub (I_H), input shaft and headset driver (I_{IN}), counter shaft with all driver and output gears "welded" on it except the unloaded gear (I_{CT}), and engaged output gear along with output shaft (I_{EO}). Relevant gear radii are defined by the headset driver gear (R_{HI}), headset driven gear on the counter shaft (R_{HO}), engaged driver gear (R_{EI}), unloaded driver gear (R_{UI}), engaged output gear (R_{EO}), and unloaded output gear (R_{UO}). Also, refer to the list of symbols for nomenclature. A 6 degree of freedom (DOF) model is chosen where the generalized displacement vector is: $\{\theta\}^T = \{\theta_F \quad \theta_H \quad \theta_{IN} \quad \theta_{CT} \quad \theta_{EO} \quad \theta_{UO}\}^T$. The linear system equations are given as follows, without any damping or forcing function terms.

$$I_F\ddot{\theta}_F + k_{C1}(\theta_F - \theta_H) = 0 \tag{1}$$

$$I_H\ddot{\theta}_H - k_{C1}(\theta_F - \theta_H) + k_S(\theta_H - \theta_{IN}) = 0 \tag{2}$$

$$I_{IN}\ddot{\theta}_{IN} - k_S(\theta_H - \theta_{IN}) + R_{HI}k_{GH}(R_{HI}\theta_{IN} + R_{HO}\theta_{CT}) = 0 \tag{3}$$

$$I_{CT}\ddot{\theta}_{CT} + R_{HO}k_{GH}(R_{HI}\theta_{IN} + R_{HO}\theta_{CT}) + R_{EI}k_{GE}(R_{EI}\theta_{CT} + R_{EO}\theta_{EO}) + R_{UI}k_{GU}(R_{UI}\theta_{CT} + R_{UO}\theta_{UO}) = 0 \tag{4}$$

$$I_{EO}\ddot{\theta}_{EO} + R_{EO}k_{GE}(R_{EI}\theta_{CT} + R_{EO}\theta_{EO}) = 0 \tag{5}$$

$$I_{UO}\ddot{\theta}_{UO} + R_{UO}k_{GU}(R_{UI}\theta_{CT} + R_{UO}\theta_{UO}) = 0\,. \tag{6}$$

Therefore, the stiffness and inertia matrices are defined as follows.

$$[K] = \begin{bmatrix} k_{C1} & -k_{C1} & 0 & 0 & 0 & 0 \\ -k_{C1} & k_{C1}+k_S & -k_S & 0 & 0 & 0 \\ 0 & -k_S & k_S + R_{HI}^2 k_{GH} & R_{HI}R_{HO}k_{GH} & 0 & 0 \\ 0 & 0 & R_{HI}R_{HO}k_{GH} & R_{HO}^2 k_{GH} + R_{EI}^2 k_{GE} + R_{UI}^2 k_{GU} & R_{EI}R_{EO}k_{GE} & R_{UI}R_{UO}k_{GU} \\ 0 & 0 & 0 & R_{EI}R_{EO}k_{GE} & R_{EO}^2 k_{GE} & 0 \\ 0 & 0 & 0 & R_{UI}R_{UO}k_{GU} & 0 & R_{UO}^2 k_{GU} \end{bmatrix} \tag{7}$$

$$[M] = diag(I_F, I_H, I_{IN}, I_{CT}, I_{EO}, I_{UO}) \tag{8}$$

In order to check the validity of the 6 degree of freedom model, an expanded 10 degree of freedom model is developed. In this expanded model, the conglomerated inertia I_{CT} term is divided into the counter shaft and various gear pairs including reverse idle and reverse gear, and the lumped parameter system is modeled accordingly. Both 6 and 10 degree of freedom models are simulated to yield undamped eigensolutions. For example, the non-zero natural frequencies (in Hz) for the third gear engaged condition are as follows: 15 (15), 959 (959), (2328), 3184 (3184), 5228 (5226), (6127), (6996), 7564 (7558), and (8328). The values in parentheses are from the expanded 10 degree of freedom linear model. The corresponding mode shapes are shown in Table 3. Since the maximum deviation of the simplified 6 degree of freedom model is less than 1% and all torsional mode shapes are well described, it is used for further analyses. Nevertheless, the LTI cannot explain the dynamic interactions that occur under impulse conditions.

NON-LINEAR MODEL

The clearance non-linearities of Figure 2 are included in the non-linear model. As shown in Figure 2a, the clutch model includes multi-staged stiffnesses and hysteresis elements. This non-linearity is a function of both relative displacement, $\delta_1 = \theta_F - \theta_H$, and relative velocity, $\dot{\delta}_1 = \dot{\theta}_F - \dot{\theta}_H$. Therefore, the clutch torque (T_c) can be divided into two parts to describe the multi-staged stiffness (T_{c1}) and multi-valued hysteresis (T_{c2}) characteristics.

$$T_c(\delta_1, \dot{\delta}_1) = T_{c1}(\delta_1) + T_{c2}(\delta_1, \dot{\delta}_1). \tag{9}$$

The following equation expresses the multi-staged stiffness characteristics.

$$T_{c1}(\delta_1) = \begin{cases} k_{c1}\phi_{11} + k_{c2}(\delta_1 - \phi_{11}), & \delta_1 > \phi_{11} \\ k_{c1}\delta_1, & -\phi_{11} \le \delta_1 \le \phi_{11} \\ -k_{c1}\phi_{11} + k_{c2}(\delta_1 + \phi_{11}), & \delta_1 < -\phi_{11} \end{cases} \quad (10\text{ a-c})$$

Here, ϕ_{11} is a transition angle, k_{c1} is the first stage stiffness, and k_{c2} is the second stage stiffness. Regarding the clutch torque from the hysteresis (T_{c2}), two cases are considered since T_{c2} depends on both δ_1 and $\dot{\delta}_1$. If the relative velocity between the flywheel and the clutch hub is greater than zero, the clutch torque follows the upper locus, and vice versa. This can be expressed by the following equations, where H_1 and H_2 describe hysteresis of the first and second stages respectively, as shown in Figure 2a.

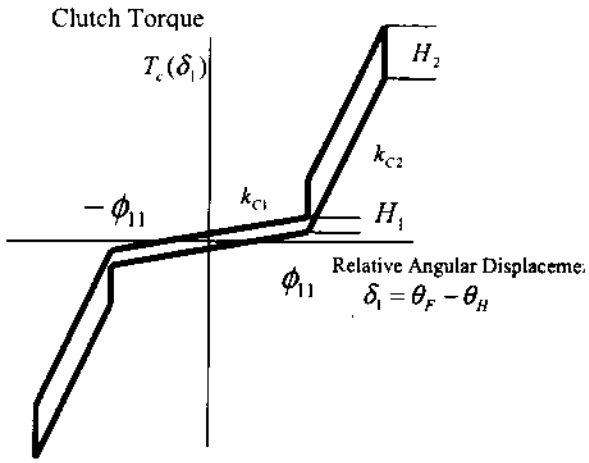

(a) Multi-staged clutch non-linearity

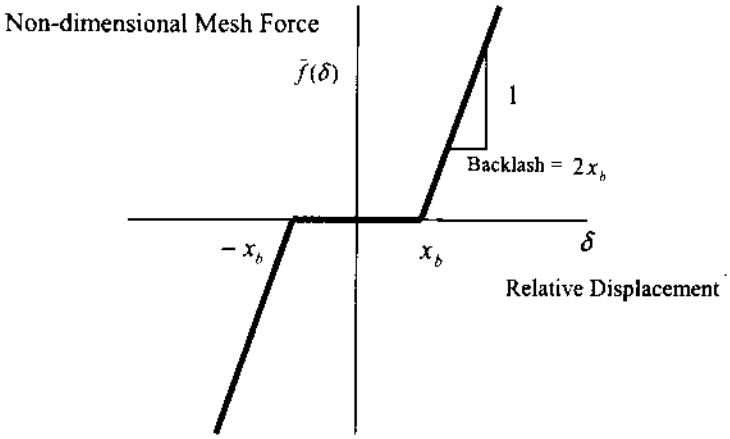

(b) Gear backlash non-linearity

Figure 2. Clearance non-linearities

$$T_{c2}(\delta_1, \dot{\delta}_1) = \begin{cases} \frac{H_2}{2} + \frac{H_2 - H_1}{2}\mathrm{sgn}(\delta_1 - \phi_{11}), & \dot{\delta}_1 > 0 \\ -\frac{H_2}{2} + \frac{H_2 - H_1}{2}\mathrm{sgn}(\delta_1 + \phi_{11}), & \dot{\delta}_1 < 0 \end{cases} \tag{11}$$

Here, the sign function is defined by the following discontinuous function.

$$\mathrm{sgn}(x) = \begin{cases} 1, & x > 0 \\ 0, & x = 0 \\ -1, & x < 0 \end{cases} \tag{11 a}$$

In order to facilitate numerical integration for the non-analytical discontinuous function, the above equation is rewritten using a continuous analytical arctangent function $\xi(x, \sigma)$ [3,6]. A "smoothening" factor (σ) in this function is used to control the error between the original discontinuous and "smoothened" continuous functions. An appropriate value of σ is obtained based on the convergence test of a numerical algorithm; note that σ

should be sufficiently high to observe impacts. The value of σ used in this paper is 10^6.

$$\mathrm{sgn}(x) \approx \xi(x,\sigma) = \frac{2}{\pi}\arctan(\sigma x) \qquad (11\ b)$$

Therefore, the sum of the clutch torques from multi-staged stiffness and hysteresis is rewritten as:

$$\begin{aligned} T_c \approx\ & k_{c2}\delta_1 + 0.5(k_{c2}-k_{c1})\{(\delta_1-\phi_{11})\xi(\delta_1-\phi_{11},\sigma) - (\delta_1+\phi_{11})\xi(\delta_1+\phi_{11},\sigma)\} \\ & + 0.5\xi(\dot{\delta}_1,\sigma)H_2 \\ & + 0.25(H_2-H_1)\{\xi(\delta_1+\phi_{11},\sigma)(1-\xi(\dot{\delta}_1,\sigma)) + \xi(\delta_1-\phi_{11},\sigma)(1+\xi(\dot{\delta}_1,\sigma))\} \end{aligned} \qquad (12)$$

Next, the gear pair regimes are modeled in terms of gear mesh stiffnesses (k_{GH}, k_{GE}, and k_{GU}), and associated backlashes ($2x_{bH}$, $2x_{bE}$, and $2x_{bU}$). The non-dimensional mesh force along the line of action is depicted in Figure 2b and expressed below using a non-analytical function. It is also rewritten using a "smoothening" function for all ranges of δ [4].

$$\bar{f}(\delta,x_b) = \begin{cases} \delta - x_b, & \delta > x_b \\ 0.0, & -x_b \le \delta \le x_b \\ \delta + x_b, & \delta < -x_b \end{cases} \qquad (13)$$

$$\bar{f}(\delta,x_b) = \delta + \frac{(\delta-x_b)\xi(\delta-x_b,\sigma) - (\delta+x_b)\xi(\delta+x_b,\sigma)}{2} \qquad (14)$$

Finally, the non-linear system equations with forcing function (T_E) and drag damping torques (T_D) are as follows. The dry friction is already included in the clearance functions.

$$I_F\ddot{\theta}_F + T_c(\delta_1,\dot{\delta}_1) = T_E(t) \qquad (15)$$

$$I_H\ddot{\theta}_H - T_c(\delta_1,\dot{\delta}_1) + k_S(\theta_H - \theta_{IN}) = 0 \qquad (16)$$

$$I_{IN}\ddot{\theta}_{IN} - k_S(\theta_H - \theta_{IN}) + R_{HI}k_{GH}\bar{f}(\delta_3,x_{bH}) = T_{D1}(t) \qquad (17)$$

$$\begin{aligned} & I_{CT}\ddot{\theta}_{CT} + R_{HO}k_{GH}\bar{f}(\delta_3,x_{bH}) + \\ & R_{EI}k_{GE}\bar{f}(\delta_4,x_{bE}) + R_{UI}k_{GU}\bar{f}(\delta_5,x_{bU}) = T_{D2(t)} \end{aligned} \qquad (18)$$

$$I_{EO}\ddot{\theta}_{EO} + R_{EO}k_{GE}\bar{f}(\delta_4,x_{bE}) = T_{D3}(t) - T_{D4}(t) \qquad (19)$$

$$I_{UO}\ddot{\theta}_{UO} + R_{UO}k_{GU}\bar{f}(\delta_5,x_{bU}) = T_{D4}(t)\,. \qquad (20)$$

Here, the rest of relative displacements are defined as: $\delta_3 = R_{HI}\theta_{IN} + R_{HO}\theta_{CT}$, $\delta_4 = R_{EI}\theta_{CT} + R_{EO}\theta_{EO}$, and $\delta_5 = R_{UI}\theta_{CT} + R_{UO}\theta_{UO}$. The engine excitation torque $T_E(t)$ time history is decomposed as follows.

$$T_E(t) = T_m + \sum_{j=1}^{24} T_{pj}\sin(j\Omega_p t + \varphi_j) \qquad (21)$$

Here, T_m is the mean engine excitation torque, T_{pj} is the excitation amplitude of j-th harmonic, Ω_p is the firing frequency corresponding to a certain engine speed, and φ_j are harmonic phase angles. The viscous drag torques, T_{D1}, T_{D2}, and T_{D3} are functions of shafts rotations and vibratory torsional velocities. They can be decomposed into mean (subscript m) and vibratory (subscript p) drag parts as expressed below. The mean parts can be easily calculated using gear radii.

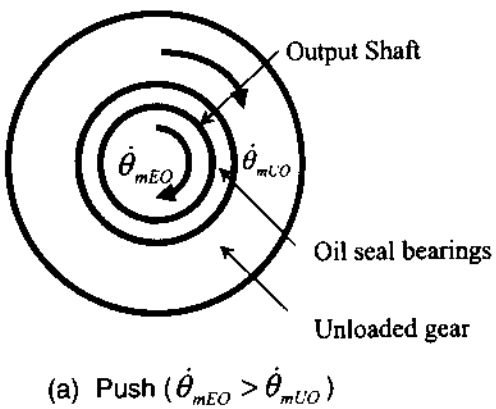

(a) Push ($\dot{\theta}_{mEO} > \dot{\theta}_{mUO}$)

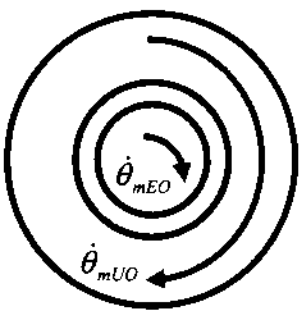

(b) Drag ($\dot{\theta}_{mEO} < \dot{\theta}_{mUO}$)

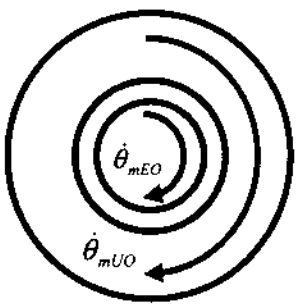

(c) Equal ($\dot{\theta}_{mEO} = \dot{\theta}_{mUO}$)

Figure 3. Relative motions between unloaded gear and output shaft

$$T_{D1}(t) = -c_{IN}\dot{\theta}_{IN}(t) = -c_{IN}\left(\dot{\theta}_{mIN} + \dot{\theta}_{pIN}(t)\right) = T_{mD1} + T_{pD1}(t) \quad (22a)$$

$$T_{D2}(t) = -c_{CT}\dot{\theta}_{CT}(t) = -c_{CT}\left(\dot{\theta}_{mCT} + \dot{\theta}_{pCT}(t)\right) = T_{mD2} + T_{pD2}(t) \quad (22b)$$

$$T_{D3}(t) = -c_{EO}\dot{\theta}_{EO}(t) = -c_{EO}\left(\dot{\theta}_{mEO} + \dot{\theta}_{pEO}(t)\right) = T_{mD3} + T_{pD3}(t) \quad (22c)$$

However, the drag torque (T_{D4}) between the unloaded gear ($_{UO}$) and output shaft ($_{EO}$) needs to be defined in terms of relative velocity terms. Therefore,

$$\begin{aligned} T_{D4}(t) &= -c_{UO}(\dot{\theta}_{UO}(t) - \dot{\theta}_{EO}(t)) \\ &= -c_{UO}\left((\dot{\theta}_{mUO} - \dot{\theta}_{mEO}) + (\dot{\theta}_{pUO}(t) - \dot{\theta}_{pEO}(t))\right) \end{aligned} \quad (23)$$

The direction of T_{D4}, as shown in Figure 3 is controlled by three conditions. First, the main shaft rotates faster than the unloaded gear. In this case, the drag actually pulls the unloaded gear along and makes it more likely to lose contact with the driving gear. Second, the converse occurs when the main shaft runs slower than the unloaded gear. Third, the main shaft and the unloaded gear rotate with the same speed. There would be no drag torque effect for this rare case.

Numerical values of clearance parameters (such as k_{C1}, k_{C2}, H_1, H_2 and x_b) are known from the component design information. Mass and stiffness matrix parameters are usually determined by running a computational model of much higher dimension [3], or from experimental modal data when available. The excitation torque time history $T_E(t)$ is usually available but the estimation of drag torques $T_{Di}(t)$ is often difficult. One must therefore rely on limited information.

Given the governing equations and mean (operating) condition, we can calculate all initial displacements and velocities for dynamic simulation. Finally, the governing equations are non-dimensionalized to ensure that the system is not strongly "stiff" [2,3]. A 4/5th order Runge-Kutta algorithm with a variable time step is used for numerical integration [3]

RESULTS

Typical results yielded by computer simulations are shown in Table 4 and Figures 4 to 6. According to Table 4, the tendency of rattle is reduced when one of the lower gears is in an unloaded position. For example, in a third gear run-up condition, the first gear rotates slower than the output shaft and it experiences the "push" type viscous drag as shown in Figure 3a. The viscous drag (T_{D4}) provides the "push" force that tries to separate the unloaded gear from contact with the driver, and this reduces the mean operating torque. The opposite happens in the case of higher gears, say either the forth or the overdrive when unloaded. These unloaded gears experience the "drag" type as in Figure 3b, since the output shaft rotates slower than these gears. As shown in Table 4, the mean operating force of unloaded first gear is 10N; compare it with 172N for the overdrive gear under the "drag" condition (note '+' markings in Figure 5). However, it is observed that the first gear when unloaded does not produce any impacts even when its mean torque is lower than that of other unloaded gears. Nevertheless, the overdrive gear when unloaded generates significant single-sided impacts. Changes in the viscous drag torque T_{D4} provide some control, but the vibro-impacts within the unloaded gear regimes are still observed. Therefore, one must pay attention to changes in the mean operating torque that are introduced by the drag torque T_{D4}.

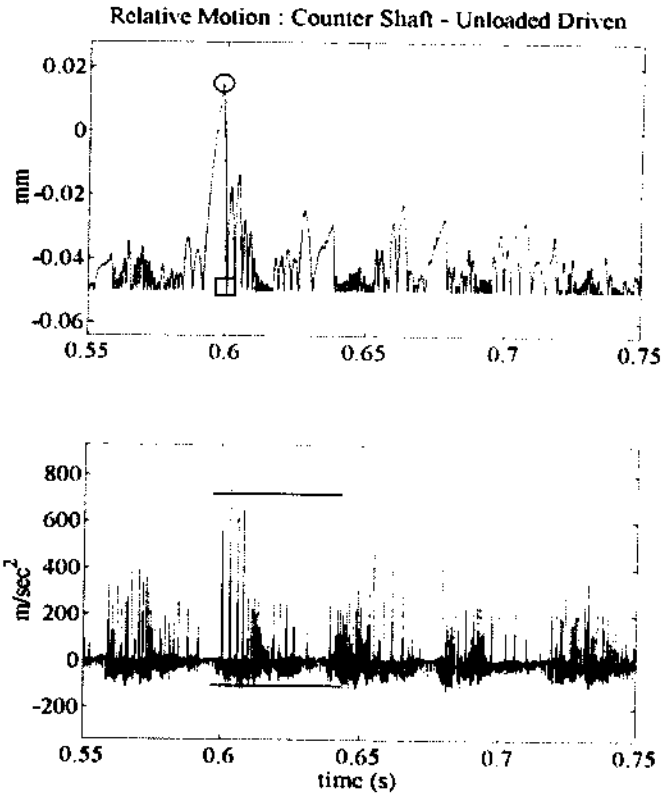

Figure 4. Relative acceleration and displacement of unloaded overdrive gear (during the 3rd gear run-up condition)

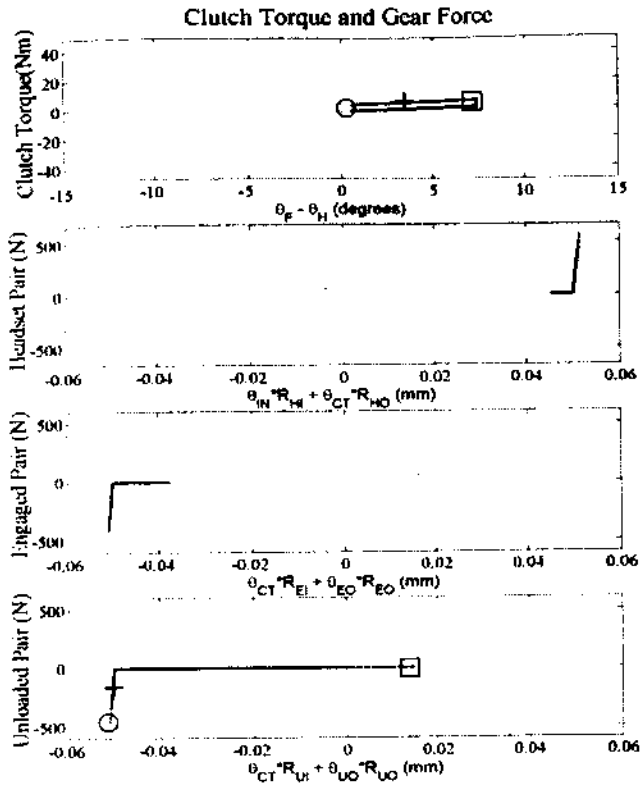

Figure 5. Clutch torque and gear mesh forces (during the 3rd gear run-up condition)

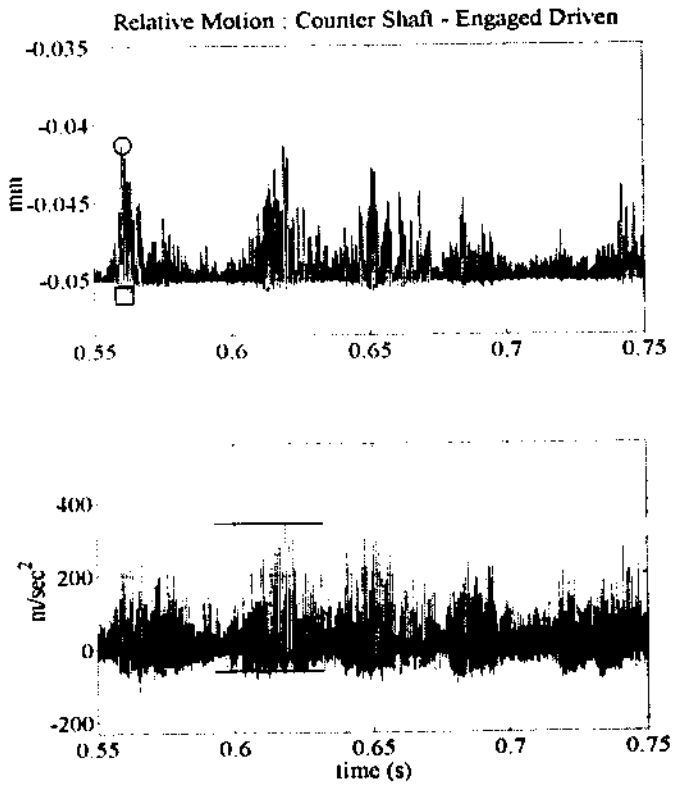

Figure 6. Relative acceleration and displacement of engaged gear pair (during the 3rd gear run-up condition)

The time domain results corresponding to Table 4 are seen in Figures 4 and 6. The full contact on the driven side, a flat regime around the -0.05 mm line, is relatively short and the unloaded driven gear instantaneously goes back to the floating condition (relative displacement plot in Figure 4). The unloaded overdrive gear floats between –0.0501 and 0.0143 mm. The maximum relative displacement from the contact point is marked in Figures 4 through 6 by a circle, and the minimum as a square. The calculated peak-to-peak relative acceleration level is 910 m/s^2 (relative acceleration plot in Figure 4), and this value is close to the measured acceleration of 863 m/s^2 (Table 1). It can also be observed in Figure 5, in terms of the clutch torque and gear force plots. Gear mesh force of the unloaded gear pair shows significant transition in the displacement. Vibro-impacts from the unloaded gear affect the engaged gear pairs, and indeed there is a sign of small impacts at the engaged and headset gear pair locations. Simulated peak-to-peak relative acceleration level at the headset pair is 245 m/s^2, and the measured value is 189 m/s^2. The impact at the engaged pair can be clearly observed in Figure 6, and tooth separations at the engaged gear pair are observed. This seems to suggest that significant single-sided impacts arising from the unloaded gear pair regime can trigger impacts within the headset or engaged pair [8]. However, the engaged pair shows the calculated relative acceleration level of 425 m/s^2 as compared to 101 m/s^2 from the experiment. This discrepancy comes from the reduced order model that treats the engaged gear and the output shaft as an inertial element, since the driveline and vehicle inertias are not considered.

After a comparison of the relative acceleration levels for both engaged and unloaded gear pairs, some physical phenomena and associated vibratory motion levels are found to be similar to those seen in vehicle measurements. It is clear that impacts from the unloaded gear pair influence the relative acceleration level of the engaged gear pair. This explains the acceleration burst of the engaged gear pair at 950 rpm, as measured in the vehicle.

EFFECT OF DRAG TORQUE DISTRIBUTION

To find possible solutions to the unloaded gear pair rattle, the effect of drag torque is studied. The simulation model of Figure 1 is examined for the baseline and modified cases. The drag torque distribution for case I is set as: drag on the input shaft (T_{D1}) =3.7%, drag on the counter shaft (T_{D2}) =70.4%, drag on the output shaft (T_{D3}) =18.5%, and drag between the unloaded gear and the output shaft (T_{D4}) =7.4%. For case II, values T_{D1} and T_{D2} are changed to 70.4% and 3.7% respectively. Case II simulates situation when the drag torque of the input shaft is larger than that of the counter shaft. For case I, clutch torque and gear mesh forces are already shown in

Figure 5. When the results from case II are presented in Figure 7, it is seen that this case is more favorable to rattle, since the single-sided impacts from the gear pairs are now double-sided impacts. The mean operating points for the clutch, engaged and unloaded gear pairs are not changed since the related drag torques are the same as before. However, the operating point at the headset gear pair is now closer to the backlash transition (gear mesh force plot in Figure 7), and it is due to reduced driven side drag torque on the counter shaft. Based on these results, it is not easy to state which gear pair, whether the headset or the unloaded, initiates the impulsive action. Nonetheless, such results from case I and II match one of the gear rattle criteria proposed by Singh et. al. [2], which states that the higher viscous drag in driven side may reduce the likelihood of rattle.

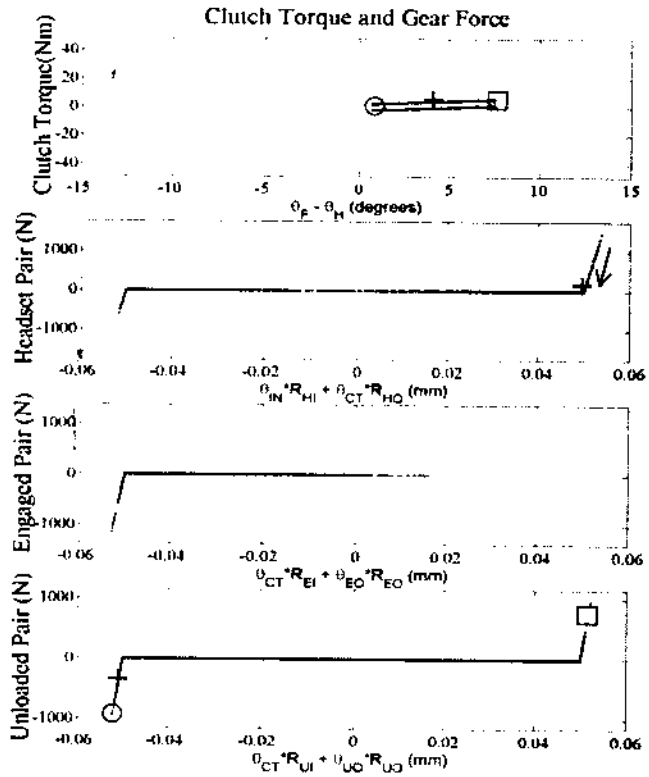

Figure 7. Clutch torque and gear mesh forces given higher drag on input

In some transmissions, the drag between the main shaft and unloaded gear is probably minimized to increase the energy efficiency. However, lower drags can initiate impact-favorable conditions when the unloaded gear is about to lose contact. A typical comparison of the relative acceleration levels and rattle conditions between low and high T_{D4} is shown in Table 5. The viscous drag coefficient c_4 is varied from 100% to 220% of its baseline value. All simulation conditions are for the third gear run-up with the overdrive being the unloaded pair. The distribution of drag torques follows case I. As demonstrated in Table 5, the lower drag cases tend to favor rattle. It is also clearly seen that unloaded gear impacts can trigger rattle within engaged and headset pairs, since vibro-impacts disappear when the unloaded pair does not initiate the impulsive action. Impacts from the engaged gear pair are eliminated first as the drag torque T_{D4} increases, but impacts from the headset pair persist unless the unloaded gear pair rattle is minimized. This is due to dramatic changes in relative acceleration of the engaged pair (from 425 to 55 m/s^2) as opposed to moderate changes in the headset pair (from 245 to 125 m/s^2), as seen in Table 5.

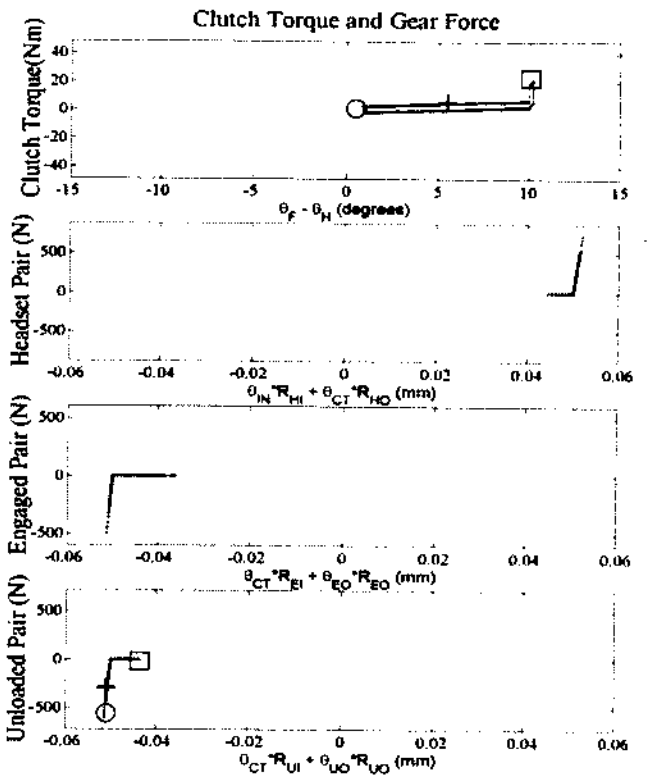

Figure 8. Clutch torque and gear mesh forces corresponding to clutch stiffness transition

Finally, the case where oil-sealed bearings are applied to each unloaded gears is considered. In this extreme case, the total drag torque of unloaded gears can be significant when compared with other cases of Table 5. The last row in Table 5 shows the results from this case. The no-impact condition suddenly turns to single-sided impacts, and separation at the headset gear is larger than those observed for other gear pairs. This phenomenon is driven by a transition in the clutch as shown in Figure 8, and it seems to trigger impacts in all of the gear pairs. Note that this case is different from the cases presented before. When the second stage is reached in the clutch, the peak-to-peak relative displacement increases dramatically as shown in Figure 8. The single-sided impacts of the clutch now transmit more fluctuations into the system. The clutch now works as an exciter rather than an isolator.

Drag torque control could be an inexpensive solution for the unloaded gear rattle problem. Adding one or two oil sealed bearings at higher gears like the third, fourth or overdrive could significantly reduce vibro-impacts. However, the impact condition is very sensitive to temperature, since the viscous drag coefficient varies with temperature. As the operating temperature rises by $20\,^{\circ}C$ from the initial condition say at $0\,^{\circ}C$, the viscous drag can be lowered by 50% of its initial value [6,7].

CONCLUSION

The reduced 6 degree of freedom non-linear model effectively shows dynamic interactions between engaged and unloaded gear pairs. Typical results from the simulation model demonstrate phenomena that are similar to those observed in vehicle experiments. A comparison of the relative acceleration levels for both engaged and unloaded gear pairs seems to suggest that significant single-sided impacts within the unloaded gear pair regime can trigger impacts within headset and engaged pairs. Simulated vibratory motions of unloaded and headset pairs are close to those measured in the vehicle environment. Yet, there is a discrepancy for the engaged pair. In order to improve prediction, equivalent inertia of the entire vehicle drivetrain must be included in the simulation model. Both inertial and drag torque distributions appear to be critical to the rattle problem, especially the viscous drag torque between the output shaft and the unloaded gear (T_{D4}). Although the drag torque control could be an inexpensive solution for the unloaded gear rattle problem, one should be aware of changes that are associated with operating temperatures as well as possible transition within the clutch. Further work is in progress that will analytically study various interactions between sub-systems.

ACKNOWLEDGMENTS

We wish to acknowledge the "gear rattle" consortium members, Eaton R & D, Eaton Clutch, Fiat CRF, LuK, Saab, and Volvo Trucks for supporting this research.

REFERENCES

1. **R. J. Comparin**, A Study of the Frequency Response of Impact pairs with Application to Automotive Gear Rattle, Ph.D Dissertation, The Ohio State University, 1988.
2. **R. Singh, H. Xie and R. J. Comparin**, Analysis of Automotive Neutral Gear Rattle, *Journal of Sound and Vibration*, Vol. 131, pp. 177-196, 1989.
3. **C. Padmanabhan, R. C. Barlow, T. E. Rook and R. Singh**, Computational Issues Associated with Gear Rattle Analysis, *Journal of Mechanical Design*, Vol. 117, pp.185-192, 1995.
4. **C. Padmanabhan, T. E. Rook and R. Singh**, Modeling of Automotive Gear Rattle Phenomenon: State of Art, Proc. of 1995 SAE Noise and Vibration Conf., pp. 669-680, paper No. 951316, Traverse City, MI.
5. **C. Padmanabhan and R. Singh**, Dynamics of a Piecewise Non-Linear System subject to Dual Harmonic Excitation Using Parametric Contribution, *Journal of Sound and Vibration* 184(5), pp.767-799. 1995
6. **E. P. Trochon**, Analytical Formulation of Automotive Drivetrain Rattle Problems, M.S. Thesis, The Ohio State University, 1997.
7. **E. P. Trochon and R. Singh**, Effect of Automotive Gearbox Temperature on Transmission Rattle Noise, NOISE-CON 98, pp. 151-156, Traverse City, MI.
8. **T. C. Kim and R. Singh**, Prediction of Rattle Noise from an Unloaded Gear Pair, *Inter-Noise 2000*, France, 2000.
9. **ROTEC user's guide**, <www.angerinc.com>

CONTACT

Web address:
<http://rclsgi.eng.ohio-state.edu/~singh/ADL.html>

LIST OF SYMBOLS

Symbols

$\delta,\dot{\delta},\ddot{\delta}$	relative displacement, velocity, and acceleration
ϕ_{11}	transition angle
φ	phase angle
$\theta,\dot{\theta},\ddot{\theta}$	absolute displacement, velocity, and acceleration
c	viscous drag coefficient
f	force
H	hysteresis
I	inertia
k	stiffness
K	general stiffness matrix
R	radius
M	inertia matrix
t	time
T	torque
$2x_b$	gear backlash

Subscripts

1, 2	stage number
C	clutch
CT	counter shaft (headset driven)
D	viscous drag
E	engine
EI, EO	engaged driver, and driven gears
F	flywheel
H	clutch hub
HI, HO	headset driver, and driven gears
IN	input shaft
m	mean
p	alternating component
S	input shaft
UI, UO	unengaged driver, and driven gears

Vehicle	Light truck (3/4 ton)
Engine	V6 Turbo Diesel
Drive Train	Rear wheel drive with two U-joints
Transmissions	5 speed with overdrive, dual-axis type (both A and B)
Sensors	3 magnetic pickups – analog type 1 triaxial accelerometer (on axle bearing)
Analyzer	ROTEC [9] Channel 1: reference speed (flywheel) Channel 2: each gear pair location on the counter shaft (driving) Channel 3: each gear pair location on the output shaft (driven)

Table 1. Vehicle and instrumentation specifications for an experimental case study

Engine Speed	Relative Acceleration $\ddot{\theta}_p$ (peak-to-peak, rad/s^2)					Noise Perception
	Engaged Pair (3rd)	Headset Pair	Unloaded Pair			
			1st	2nd	Overdrive	
850 rpm	500	1000	800	900	2300	No Rattle
950 rpm	1800 (101 m/s^2)	2000 (189 m/s^2)	1300	2400	5000 (863 m/s^2)	Severe Rattle

Table 2. Relative acceleration levels from the vehicle (A) run-up experiments. Numbers within the parentheses are corresponding translational accelerations, where available.

Vibration Mode	1	2	3	4	5
Natural Frequency (Hz)	15	959	3184	5228	7564
Normalized Modal Displacements					
Flywheel (θ_F)	-0.007	0.000	0.000	0.000	0.000
Clutch Hub (θ_H)	0.999	1.000	-0.010	-0.001	0.000
Headset Driver and Input Shaft (θ_{IN})	1.000	-0.850	1.000	0.206	0.002
Headset Driven Counter Shaft + Other Gears (θ_{CT})	1.000	-0.973	-0.142	-0.165	0.023
Engaged (Loaded) Gear + Output Shaft (θ_{EO})	1.000	-0.987	-0.512	1.458	0.004
Unengaged (Unloaded) Gear (θ_{UO})	1.000	-0.975	-0.158	-0.197	1.124

Table 3. Natural frequencies and mode shapes of the 6 degree of freedom linear model of Figure 1, in the third gear engaged condition.

Unloaded Gear	Inertia I_{UO} (kg/m^2)	Gear Mesh Force $\bar{f}(\delta)$ (N)			Relative Displacement (δ) (mm)		Impact Condition
		Mean	Maximum	Minimum	Minimum	Maximum	
1st	4.000e-4	10	20	0	-0.0501	-0.0500	None
2nd	3.500e-4	50	190	0	-0.0501	-0.0436	Single-Sided
Overdrive	2.000e-4	172	436	0	-0.0501	-0.0143	Single-Sided

Table 4. Gear mesh forces and relative displacements of unloaded gears, in the third gear engaged condition. Here, $x_b = 0.05mm$.

Drag Torque (T_{D4})	Clutch Motion		Impact Conditions and Relative Accelerations (m/s^2)		
	Mean δ_{ml} (degree)	Dynamic Range $\Delta\delta_{lp}$ (degree)	Unloaded Pair	Engaged Pair	Headset Pair
100 % (Baseline)	3.97	0.59 - 7.35	Single-Sided 910	Single-Sided 425	Single-Sided 245
150 %	4.08	0.72 - 7.45	Single-Sided 535	Single-Sided 305	Single-Sided 245
200 %	4.27	0.90 – 7.65	Single-Sided 155	None 55	Single-Sided 125
220 %	4.32	0.96 – 7.68	None 0.6	None 1.1	None 4.0
1000 %	6.04	1.92 – 10.17 (transition)	Single-Sided 475	Single-Sided 525	Single-Sided 295

Table 5. Summary of the effects of drag torque T_{D4}.